Geng *et al.*
Chinese Journal of Mechanical Engineering (2024) 37:115
https://doi.org/10.1186/s10033-024-01112-7

Chinese Journal of Mechanical Engineering

ORIGINAL ARTICLE

Open Access

New Multi-Channel VSMFxLMS Algorithm for Vibration Reduction of Gear Systems

Zhibo Geng[1], Min Chen[1,2*], Yingjian Wang[1], Yun Kong[3] and Ke Xiao[4]

Abstract

At present, the active control of gear vibration mostly relies on existing algorithms. In order to achieve effective vibration reduction of the gear system, particularly during the vibration process, this paper proposes a multi-channel VSMFxLMS algorithm based on the FxLMS algorithm. This novel approach takes into account the time-varying nature of the vibration signal during gear vibration. Adaptive filter power coefficients are updated in a skip-tongue variable-step manner using momentum factors. Firstly, the paper establishes the dynamics model of the gear system and analyzes the nonlinear dynamic characteristics of the system. It then examines the vibration damping effect of the FxLMS algorithm and analyzes its performance under different gear system motion states, considering different step lengths and momentum factors. Lastly, the proposed VSMFxLMS algorithm is compared with the FxLMS algorithm, highlighting the superiority of the former. Overall, this research highlights the potential of a multi-channel VSMFxLMS algorithm in reducing vibrations in gear systems. The study optimizes the performance of gear systems while using advanced control strategies.

Keywords Vibration reduction, Gear system, FxLMS algorithm, Multi-channel VSMFxLMS algorithm

1 Introduction

Gears play a vital role in the transmission system and are widely used for their numerous benefits. However, gear vibration is a common issue that affects their optimal operation. The vibrations generated during gear operation can result in excessive wear and damage, undermining the performance and reliability of the gear system. The causes of gear vibration are multifaceted and can be due to unbalanced loads, design or manufacturing errors, or improper gear alignment. Managing gear vibration is crucial for enhancing gear system's performance, durability, and efficiency. By implementing appropriate measures, gear systems can be optimized for better performance and long-term reliability.

To effectively control vibrations, Richards et al.[1] suggested a passive approach based on gear mesh contact, whereby a periodic structural component was implemented to attenuate the transmitted vibrations as well as the excitation forces. Hui et al. [2] developed a mesh stiffness model for profile shifted gears with addendum and tooth profile modifications to reduce vibrations. Xiao et al. [3–5] developed an energy dissipation model to minimize the vibration of mechanical systems under centrifugal loads, particularly in harsh conditions. The model utilized powder materials for their damping properties, with their size found to significantly impact the vibration characteristics. The study revealed that properly selected powder damping materials could effectively dampen vibrations and reduce the negative effects of mechanical jarring. A meshing stiffness model was proposed by Yu et al. [6] to study the influence of the addendum modification on the dynamic response of the gear system. Wei

*Correspondence:
Min Chen
chenmin@uestc.edu.cn
[1] School of Aeronautics and Astronautics, University of Electronic Science and technology of China, Chengdu 611731, China
[2] Yangtze Delta Region Institute, University of Electronic Science and Technology of China, Huzhou 313000, China
[3] School of Mechanical Engineering, Bejing Institute of Technology, Beijing 100081, China
[4] College of Mechanical and Vehicle Engineering, Chongqing University, Chongqing 400044, China

© The Author(s) 2024. **Open Access** This article is licensed under a Creative Commons Attribution 4.0 International License, which permits use, sharing, adaptation, distribution and reproduction in any medium or format, as long as you give appropriate credit to the original author(s) and the source, provide a link to the Creative Commons licence, and indicate if changes were made. The images or other third party material in this article are included in the article's Creative Commons licence, unless indicated otherwise in a credit line to the material. If material is not included in the article's Creative Commons licence and your intended use is not permitted by statutory regulation or exceeds the permitted use, you will need to obtain permission directly from the copyright holder. To view a copy of this licence, visit http://creativecommons.org/licenses/by/4.0/.

et al. [7] analyzed the dynamic behavior of a planetary gear system with a flexible structure. And they [8] developed a model for tooth modification which aimed at reducing vibration. The model determined optimal values of the tooth modification parameters to minimize vibration amplitude. Ref. [9] introduces a mechanical model for a vibration isolation system consisting of an Integral elastic ring squeeze film damper and elastic damping supports for gear systems. Samani et al. [10] analyzed the nonlinear vibration of a spiral bevel gear pair with a new model of tooth modification. Wang [11] proposed a multi-objective modification optimal design method for helical gears, aimed at reducing vibration and noise. A novel type of cylindrical spur gear is proposed by Jiang and Liu [12], which utilizes elastic isolation to reduce vibration. The gear system consists of three parts—the gear body, elastic isolation layer, and involute tooth shape body. Chen et al. [13] proposed a high-order phasing gear to reduce the fluctuation of mesh stiffness and thus control the vibration of the gear system.

With the advancement of computer technology, active vibration damping technology has become increasingly prevalent in gear systems. Active vibration damping technology offers numerous benefits, including improved gear operation, reduced noise levels, increased reliability, and reduced maintenance costs. In order to reduce torsional vibrations, Gill-Jeong [14] added a unidirectional clutch in the gear transmission system. Gao et al. [15] considered online identification and filtering functions in the Filtered-x Least Mean Square (FxLMS) algorithm. The results show that the method is more effective in damping vibration than the traditional FxLMS algorithm, but the response time is somewhat prolonged. Spada and Nicoletti [16] discussed the application of Udwadia-Kalaba methodology in active vibration control. To mitigate the negative impact of meshing stiffness, Dogruer and Pirsoltan [17] proposed a nonlinear controller that modifies the torque applied to the driving gear. Sun et al. [18] developed a built-in active vibration control structure for multistage gearboxes based on modal results from finite element solutions. Wang et al. [19] presented an adaptive fuzzy proportion integration differentiation control algorithm to reduce the vibration, and analyzed the effect of vibration frequency control via experiment. Based on FxLMS algorithm, Philipp et al. [20] proposed a novel PENSE algorithm to reduce the vibration of the gear transmission system. Based on the PID controller, Sheng et al. [21] studied the effect of controller on the vibration reduction of a semi-direct gear system. A novel lattice recursive least square (NLRLS) algorithm was suggested by Luo et al. [22], which has a fast convergence speed and is sensitive to frequency changes. A surface-active modification method proposed by Peng and Zhou [23] is proposed to decrease the vibration of the face gear drive. The results showed that the vibration is reduced after the optimization. A novel active vibration suppression structure for a multistage gear system with a built-in piezoelectric actuator has been designed to generate active control force. An active controller has been designed and implemented utilizing the FxLMS adaptive algorithm [24]. Majumder and Tiwari [25] proposed a method of using active magnetic bearings to suppress vibrations in gear systems, and conducted experimental verification. Olanipekun et al. [26] proposed active control of force and power through a rotating frame to reduce gear system vibration.

Active vibration damping technology provides an effective means of reducing vibration in gear systems. It offers numerous benefits and can be particularly useful in challenging operating environments. Currently, there is relatively less research on active damping of gear systems compared to research on passive damping. Moreover, the application of algorithms is not extensively explored, and the optimization effect of existing algorithms is limited. Active vibration reduction optimization algorithms often do not prioritize the effectiveness of damping and the speed of convergence. To address this issue, this paper proposes a multi-channel Variable step size FxLMS algorithm with momentum (VSMFxLMS) algorithm based on the FxLMS algorithm. This algorithm involves updating the adaptive filter power coefficients using a skip-tongue line variable-step method and momentum factors. The results of the study demonstrate that this algorithm can effectively suppress while maintaining the convergence speed gear vibration when compared to the FxLMS algorithm.

2 Methodology

2.1 The Meshing Force and Friction

The meshing force of the gear pair can be expressed as

$$F_{mi} = k_{mi} f(Y) + 0.5 c_{mi} \dot{Y} \quad (i = 1,\ 2), \tag{1}$$

where k_{mi} and c_{mi} respectively denote the meshing stiffness and damping of the ith tooth pair, which are obtained in Ref. [27]; Y is the dynamic transmission error, which can be expressed as

$$Y = y_1 - y_2 + \theta_1 r_{b1} + \theta_2 r_{b2} - e(t), \tag{2}$$

where subscripts 1 and 2 denote the driving gear and driven gear, respectively; y denotes the vibration displacement in y direction; θ is the angular vibration displacement of the driving gear and driven gear, respectively; r_b is the radius of the basic circle; $e(t)$ is the static transmission error.

The gear backlash function can be represented as

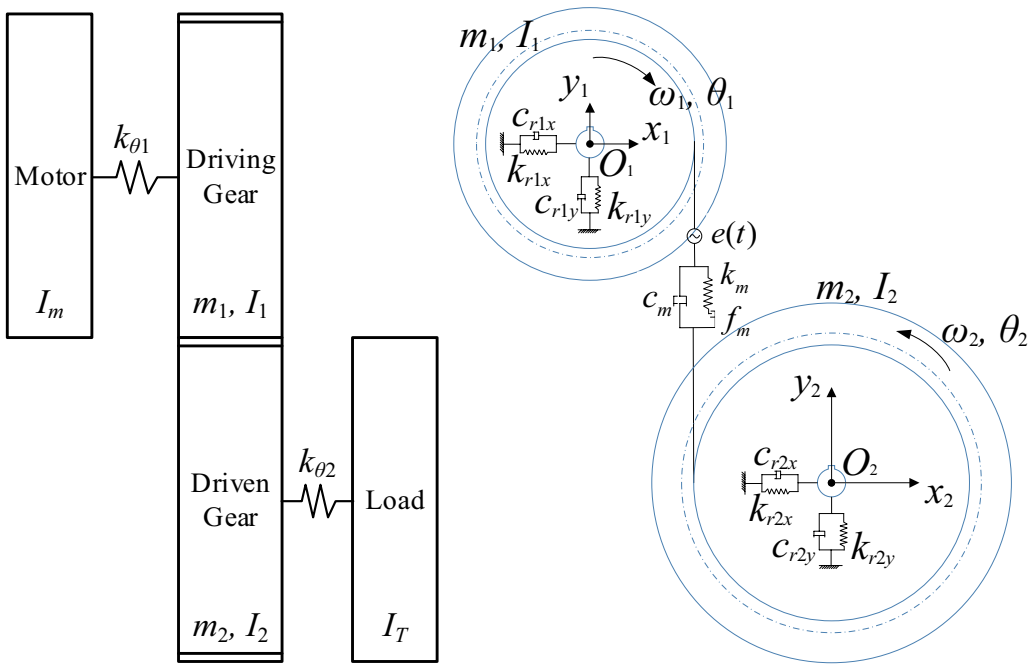

Figure 1 Dynamic model of the gear transmission system

$$f_{mi}(Y) = \begin{cases} Y - b_h, & Y > b_h, \\ 0, & -b_h \le Y \le b_h, \\ Y + b_h, & Y < -b_h, \end{cases} \tag{3}$$

where the total gear backlash is $2b_h$.

The friction force is given as

$$F_{fi} = \mu_i \lambda_i F_{mi}, \quad (i = 1,\ 2), \tag{4}$$

where λ_i and μ_i respectively denote the directional coefficient and friction coefficient of the tooth surface, which can be calculated by Ref. [27].

The friction arms of the gear pair can be derived as

$$\begin{cases} L_{11} = a\sin\alpha - \sqrt{r_{a2}^2 - r_{b2}^2} + r_{b1}\omega_1 t_1, \\ L_{12} = a\sin\alpha - \sqrt{r_{a2}^2 - r_{b2}^2} + r_{b1}\omega_1 t_2, \\ L_{21} = \sqrt{r_{a2}^2 - r_{b2}^2} - r_{b1}\omega_1 t_1, \\ L_{22} = \sqrt{r_{a2}^2 - r_{b2}^2} - r_{b1}\omega_1 t_2, \end{cases} \tag{5}$$

where L_{1i} and L_{2i} respectively denote friction arms between ith tooth pair; a represents the center distance of the gear pair; w is the angular velocity; t_i is the meshing time of the ith tooth pair; r_{a2} is the addendum circle of the driving gear.

2.2 The Nonlinear Dynamic Model

The lumped massed model of the gear transmission system is shown in Figure 1. It is a simplified bending-torsional coupling model with eight degrees of freedom. The parameters of the gear transmission system are marked in Figure 1.

The dynamic model of the gear transmission system is given in Eq. (6). In Eq. (6), subscripts m and T respectively denote the motor and load; I and m respectively denote the moment of inertia and mass; x is the vibration displacement in x direction; k_r and c_r represent the supporting stiffness and supporting damping, respectively; T is the torque.

$$\begin{cases} I_m\ddot{\theta}_m = T_m - k_{\theta 1}(\theta_m - \theta_1) - c_{\theta 1}(\dot{\theta}_m - \dot{\theta}_1), \\ m_1\ddot{x}_1 + c_{r1x}\dot{x}_1 + k_{r1x}f_{1bm}(x_1) = -(F_{f1} + F_{f2}), \\ m_1\ddot{y}_1 + c_{r1y}\dot{y}_1 + k_{r1y}f_{1bm}(y_1) = -(F_{m1} + F_{m2}), \\ I_1\ddot{\theta}_1 = -(F_{m1} + F_{m2}) \cdot r_{b1} - (F_{f1}L_{11} + F_{f2}L_{12}) \\ \qquad + k_{\theta 1}(\theta_m - \theta_1) + c_{\theta 1}(\dot{\theta}_m - \dot{\theta}_1), \\ m_2\ddot{x}_2 + c_{r2x}\dot{x}_2 + k_{r2x}f_{2bm}(x_2) = F_{f1} + F_{f2}, \\ m_2\ddot{y}_2 + c_{r2y}\dot{y}_2 + k_{r2y}f_{2bm}(y_2) = F_{m1} + F_{m2}, \\ I_2\ddot{\theta}_2 = -(F_{m1} + F_{m2}) \cdot r_{b2} - (F_{f1}L_{21} + F_{f2}L_{22}) \\ \qquad - k_{\theta 2}(\theta_2 - \theta_T) - c_{\theta 2}(\dot{\theta}_2 - \dot{\theta}_T), \\ I_T\ddot{\theta}_T = -T_T + k_{\theta 2}(\theta_2 - \theta_T) + c_{\theta 2}(\dot{\theta}_2 - \dot{\theta}_T). \end{cases} \tag{6}$$

The non-dimensional time τ used in the analysis can be defined as $\tau = w_n t$, where w_n is the natural frequency

of the gear pair. The natural frequency can be calculated using the expression $w_n = (k_n / m_{eq})^{1/2}$, in which m_{eq} is the equivalent mass of the gear pair and k_n is the average value of the meshing stiffness. To facilitate the calculations, a nominal displacement scale, b_c, is also introduced. Using these parameters, the non-dimensional parameters can be determined as follows:

$\eta_{m1}=k_{\theta1}/I_m w_n^2$, $\xi_{m1}=c_{\theta1}/I_m w_n$, $\xi_{r1x}=c_{r1x}/m_1 w_n$, $\xi_{r1y}=c_{r1y}/m_1 w_n$, $\xi_1=\xi_2=c_m/m_1 w_n$, $\xi_3=\xi_4=c_m r_{b1}/I_1 w_n$, $\eta_{r1x}=k_{r1x}/m_1 w_n^2$, $\eta_{r1y}=k_{r1y}/m_1 w_n^2$, $\eta_1=k_{m1}/m_1 w_n^2$, $\eta_2=k_{m2}/m_1 w_n^2$, $\eta_3=k_{m1} r_{b1}/I_1 w_n^2$, $\eta_4=k_{m2} r_{b1}/I_1 w_n^2$, $\eta_{m2}=k_{\theta1}/I_1 w_n^2$, $\xi_{m2}=c_{\theta1}/I_1 w_n$, $\eta_5=k_{m1}/m_2 w_n^2$, $\eta_6=k_{m2}/m_2 w_n^2$, $\xi_5=\xi_6=c_m/m_2 w_n$, $\eta_7=k_{m1} r_{b2}/I_2 w_n^2$, $\eta_8=k_{m2} r_{b2}/I_2 w_n^2$, $\xi_7=\xi_8=c_m r_{b2}/I_2 w_n$, $\xi_{r2x}=c_{r2x}/m_2 w_n$, $\xi_{r2y}=c_{r2y}/m_2 w_n$, $\eta_{r2x}=k_{r2x}/m_2 w_n^2$, $\eta_{r2y}=k_{r2y}/m_2 w_n^2$, $\eta_{m3}=k_{\theta2}/I_2 w_n^2$, $\xi_{m3}=c_{\theta2}/I_2 w_n$, $\eta_{m4}=k_{\theta2}/I_T w_n^2$, $\xi_{m4}=c_{\theta2}/I_T w_n$, $f_1=T_m/I_m b_c w_n^2$, $f_2=T_T/I_T b_c w_n^2$.

Therefore, Eq. (6) can be expressed as

$$\begin{cases} \ddot{q}_0 = f_1 - \eta_{m1}(q_0 - q_3) - \xi_{m1}(\dot{q}_0 - \dot{q}_3), \\ \ddot{q}_1 = -(\mu_1\lambda_1\eta_1 + \mu_2\lambda_2\eta_2) f_m(q) - (\mu_1\lambda_1 + \mu_2\lambda_2)\xi_1\dot{q} - \xi_{r1x}\dot{q}_1 - \eta_{r1x} q_1, \\ \ddot{q}_2 = -(\eta_{m1} + \eta_{m2}) f_m(q) - \xi_{m1}\dot{q} - \xi_{r1y}\dot{q}_0 - \eta_{r1x} q_0, \\ \ddot{q}_3 = -(\eta_{m3} + \eta_{m4}) f_m(q) - \xi_{m3}\dot{q} - (\mu_1\lambda_1 L_{11}\eta_{m3} + \mu_2\lambda_2 L_{12}\eta_{m4}) f_m(q)/r_{bp} \\ \qquad - (\mu_1\lambda_1 L_{11} + \mu_2\lambda_2 L_{12})\xi_{m3}\dot{q}/r_{bp} + \eta_{m2}(q_0 - q_3) + \xi_{m2}(\dot{q}_0 - \dot{q}_3), \\ \ddot{q}_4 = (\mu_1\lambda_1\eta_{m5} + \mu_2\lambda_2\eta_{m6}) f_m(q) + (\mu_1\lambda_1 + \mu_2\lambda_2)\xi_{m5}\dot{q} - \xi_{r2x}\dot{q}_4 - \eta_{r2x} q_4, \\ \ddot{q}_5 = (\eta_{m5} + \eta_{m6}) f_m(q) + \xi_{m5}\dot{q} - \xi_{r2y}\dot{q}_4 - \eta_{r2x} q_4, \\ \ddot{q}_6 = -(\eta_{m7} + \eta_{m8}) f_m(q) - \xi_{m7}\dot{q} - (\mu_1\lambda_1 L_{21}\eta_{m7} + \mu_2\lambda_2 L_{22}\eta_{m8}) f_m(q)/r_{bg} \\ \qquad - (\mu_1\lambda_1 L_{21} + \mu_2\lambda_2 L_{22})\xi_{m7}\dot{q}/r_{bg} - \eta_{m3}(q_6 - q_7) - \xi_{m3}(\dot{q}_6 - \dot{q}_7), \\ \ddot{q}_7 = -f_2 + \eta_{m4}(q_6 - q_7) + \xi_{m4}(\dot{q}_6 - \dot{q}_7), \end{cases} \tag{7}$$

where q is the dimensionless vibration displacement (or angular vibration displacement), subscripts 0–7 correspond to I_m-I_T, respectively. The gear backlash function presented in Eq. (3) can be expressed as follows.

$$f_m(q) = \begin{cases} q - (b_m + \frac{d_w}{2})/b_c, & q > (b_m + \frac{d_w}{2})/b_c, \\ 0, & (b_m + \frac{d_w}{2})/b_c \le q \le (b_m + \frac{d_w}{2})/b_c, \\ q + (b_m + \frac{d_w}{2})/b_c, & q < (b_m + \frac{d_w}{2})/b_c, \end{cases} \tag{8}$$

The parameters are shown in Table 1.

Table 1 Parameters of the gear pair

	Driving gear	Driven gear
Number of teeth	27	55
Modulus (mm)	2.5	
Pressure angle (°)	20	
Mass (kg)	0.584	2.007
Rotational inertia (kg/m^2)	0.00043	0.005487
Contact ratio	1.7002	

2.3 Active Control Algorithm for the Gear System

Based on the vibration characteristics of gear transmission systems, there are two main types of active vibration control: controlling torsional vibration and controlling bending vibration. Actuators are arranged in the circumferential and radial directions, respectively, to generate control forces that suppress the internal excitation of the gear train, resulting in reduced vibration and noise of the entire system. In this paper, the structure illustrated in Figure 2 is adopted, which utilizes an actuator that exerts control force on the shaft through additional bearings to suppress bending vibration of the shaft. This not only decreases internal excitation between the gears, but also effectively mitigates the vibration transmitted to the gearbox. This approach employs a simpler radial arrangement of the actuator, which is easier to implement in engineering compared to the circumferential arrangement.

2.3.1 Design of Multi-channel VSMFxLMS Algorithm

In this paper, we present a multi-channel VSMFxLMS algorithm as an extension to the traditional FxLMS algorithm. This algorithm is applied in parallel with an adaptive filter using the FxLMS algorithm to perform active damping of the gear system. Based on this, a multi-channel VSMFxLMS algorithm is developed. Figure 3 depicts the structure of this multi-channel VSMFxLMS active damping algorithm, and its single channel includes an active vibration reduction system based on the trap FxLMS algorithm and another based on the FxLMS algorithm. It is worth noting that while the active vibration reduction system based on the trap FxLMS algorithm does not require a reference

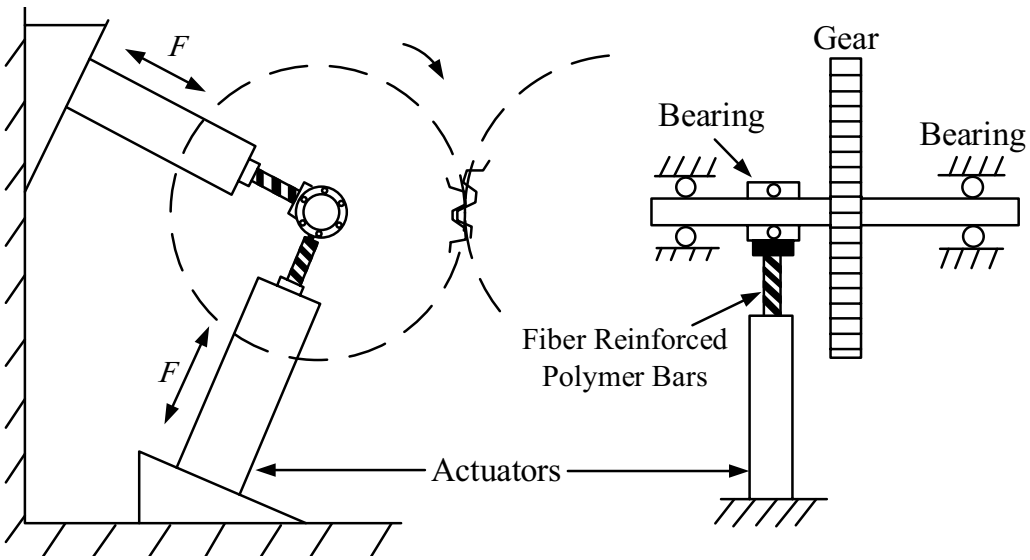

Figure 2 The active control structure of the gear transmission system

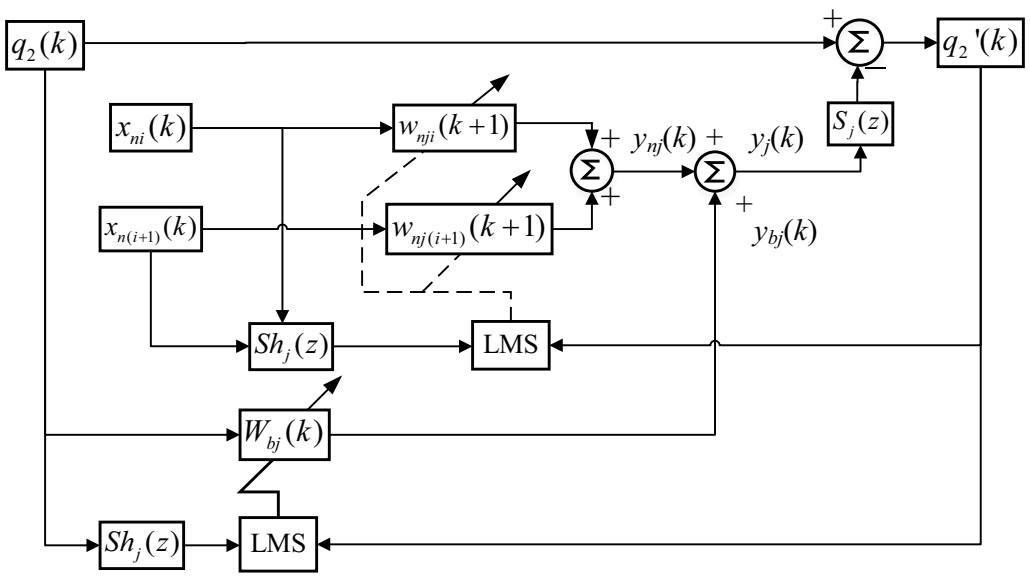

Figure 3 Diagram of multi-channel VSMFxLMS algorithm

vibration signal for acquisition, the FxLMS algorithm still requires the input of a reference vibration signal.

In Figure 3, $x_{ni}(k)$ and $x_{n(i+1)}(k)$ are the reference signals used in the notch LMS algorithm, and their expressions are as follows:

$$\begin{cases} x_{ni}(k) = A\sin(2\pi fit), \\ x_{n(i+1)}(k) = A\cos(2\pi fit), \end{cases} i = 1, 2, \cdots, m, \tag{9}$$

where m is the number of filter bands.

In Figure 3, $Sh_j(z)$ represents filter coefficients obtained after modeling the j-th secondary channel. It is used by both the FxLMS algorithm and the multiband notch LMS algorithm, with each using a different adaptive filter $W_b(k)$ and $W_n(k)$, respectively; q_2' is the vibration displacement after algorithm optimization. The adaptive filter order used by the FxLMS algorithm will be determined based on the specific situation, while the adaptive filter order used by the multiband notch FxLMS algorithm is fixed at $2i$. The higher the filter order used by the FxLMS algorithm, the better the noise reduction effect, but also correspondingly increased computational complexity. Therefore, the selection of the filter order should

consider the noise reduction performance and hardware computing speed.

$y_{bj}(k)$ and $y_{nj}(k)$ represent the outputs of the FxLMS and multiband notch LMS algorithms, respectively, for the j-th channel. Their expressions are as follows:

$$\begin{cases} y_{bj}(k) = q_2^{\mathrm{T}}(k)W_{bj}(k), \\ y_{nj}(k) = \sum_{i=1}^{m}(x_{ni}(k)w_{nji}(k) + x_{n(i+1)}(k)w_{nj(i+1)}(k)). \end{cases} \tag{10}$$

The vibration displacement after algorithm optimization can be expressed as:

$$q_2'(k) = q_2(k) - y_j(k) * S_j(z), \tag{11}$$

where, $y_j(k)=y_{bj}(k)+y_{nj}(k)$.

The update formula for filter coefficients of the FxLMS algorithm in the j-th channel of a multichannel vibration reduction system is:

$$w_{bj}(k+1) = w_{bj}(k) - 2\mu q_2'(k)x_{bw}(k), \tag{12}$$

where, $x_{bw}(k)=y_{bj}(k)\times Sh(z)$.

The update formula for filter coefficients of the multiband notch LMS algorithms in the j-th channel is:

$$\begin{cases} w_{nji}(k+1) = w_{nji}(k) - 2\mu q_2'(k)x_{niw}(k), \\ w_{nj(i+1)}(k+1) = w_{nj(i+1)}(k) - 2\mu q_2'(k)x_{n(i+1)w}(k), \end{cases} \tag{13}$$

where, $x_{niw}(k)=x_{ni}(k)\times Sh(z)$, $x_{n(i+1)w}(k)=x_{n(i+1)}(k)\times Sh(z)$.

2.3.2 Convergence Speed and Steady-State Error Optimization of the VSMFxLMS Algorithm

In FxLMS algorithm, the step size has an important impact on the final noise reduction effect of the algorithm. Generally, for the FxLMS algorithm, the larger the step size during iteration, the faster the convergence speed, but the steady-state error will also be larger; the smaller the step size during iteration, the smaller the steady-state error, but the convergence speed will decrease accordingly. The convergence speed and steady-state error of the algorithm have a certain trade-off relationship when the step size is fixed, both of which have an impact on the final noise reduction effect: the faster the convergence speed of the algorithm, the corresponding stability will be improved to a certain extent, which is manifested in the fact that the algorithm can quickly return to the steady-state when the reference microphone receives certain interference and significant outliers; the smaller the steady-state error of the algorithm, the smaller the residual noise and the lower the sound pressure level. Using variable step size can effectively improve the performance of the FxLMS algorithm. Therefore, it is necessary to use appropriate means to modify the step size of the algorithm.

Considering that the computational cost of the algorithm should not be too high, we choose to control the step size based on the variation of the versiera function to reduce the computational complexity. Based on the standard versiera function, the error $q_2'(n)$ is used as the input variable, and the iteration step size is as follows:

$$\mu(n) = \beta(1 - \frac{1}{1+\alpha q_2'^2(n)}). \tag{14}$$

The constants α and β are both greater than 0. α has a more significant effect on the speed of step size change, while β has a larger influence on the upper limit of the step size. Since only the error signal at one moment is used, it means that the effectiveness of this step size optimization method will rely heavily on the accuracy of the error sensor. If the error sensor is disturbed by external factors at a certain moment, it will have a certain impact on the performance of the algorithm. At the same time, the farther away the error signal from the current moment, the lower its timeliness, and it should have a smaller impact on the step size at the current moment. To improve the stability of the step size optimization method and enhance the timeliness of the algorithm, the following formula is proposed as

$$\mu(m) = \beta(1 - \frac{1}{1+\alpha\sum_{l=1}^{L}\frac{l}{L}q_2'^2(l)}). \tag{15}$$

The variable step size method proposed in this paper no longer uses the value of a single error signal, but processes the error signal in blocks, using the sum of squared error signals within a period of time as the basis for step size change. At the same time, considering that the closer the moment is to the current moment, the greater the weight of the error signal in the step size change, the value of l/L in the formula is used as the weight of the error signal at that moment, which improves the effectiveness of the step size optimization method.

Since α and β are both fixed values, the step size change is relatively inflexible. Therefore, this paper introduces a momentum factor to further accelerate the convergence of the algorithm [28]. The multi-frequency notch filter FxLMS algorithm takes the instantaneous squared error $J(n)=q_2'^2(n)$ as the objective function, and uses the steepest descent method to derive the iteration formula. After introducing the momentum factor, the objective function becomes:

$$J(n)=\sum_{j=1}^{n}\eta_i^{n-j}q_2'^2(j), \tag{16}$$

where $q_2'(j)$ represents the error at time j, and η_i is the momentum factor, where $-1<\eta<1$. The iteration formula under the momentum factor is as follows:

$$\begin{cases} w_i(n+1)=w_i(n)-\dfrac{1}{2}\mu_i\nabla_{w_i}J(n), \\ w_{i+1}(n+1)=w_{i+1}(n)-\dfrac{1}{2}\mu_i\nabla_{w_{i+1}}J(n), \end{cases} \tag{17}$$

where, $\mu_i=\mu_m$. Therefore, the gradient expression at time n can be obtained as:

$$\begin{cases} \nabla_{w_i}J(n)=-2\sum_{j=1}^{n}\eta_i^{n-j}q_2'(j)x_{iw}(j), \\ \nabla_{w_{i+1}}J(n)=-2\sum_{j=1}^{n}\eta_i^{n-j}q_2'(j)x_{(i+1)w}(j). \end{cases} \tag{18}$$

Therefore, the following equation can be derived as

$$\begin{cases} w_i(n+1)=w_i(n)+\mu_i q_2'(n)x_{iw}(n) \\ \qquad +\mu_i\sum_{j=1}^{n-1}\eta_i^{n-j}q_2'(j)x_{iw}(j), \\ w_{i+1}(n+1)=w_{i+1}(n)+\mu_i q_2'(n)x_{(i+1)w}(n) \\ \qquad +\mu_i\sum_{j=1}^{n-1}\eta_i^{n-j}q_2'(j)x_{(i+1)w}(j). \end{cases} \tag{19}$$

Similarly, we can obtain

$$\begin{cases} w_i(n)=w_i(n-1)+\dfrac{\mu_i}{\eta_i}[\sum_{j=1}^{n-1}\eta_i^{n-j}q_2'(j)x_{iw}(j)], \\ w_{i+1}(n)=w_{i+1}(n-1)+\dfrac{\mu_i}{\eta_i}[\sum_{j=1}^{n-1}\eta_i^{n-j}q_2'(j)x_{(i+1)w}(j)], \end{cases} \tag{20}$$

which can be rewritten as

$$\begin{cases} \eta_i(w_i(n)-w_i(n-1))=\mu_i[\sum_{j=1}^{n-1}\eta_i^{n-j}q_2'(j)x_{iw}(j)], \\ \eta_i(w_{i+1}(n)-w_{i+1}(n-1))=\mu_i[\sum_{j=1}^{n-1}\eta_i^{n-j}q_2'(j)x_{(i+1)w}(j)]. \end{cases} \tag{21}$$

The weight coefficient update formula of the algorithm is

$$\begin{cases} w_i(n+1)=w_i(n)-2\mu_i q_2'(n)x_{iw}(n) \\ \qquad +\eta_i[w_i(n)-w_i(n-1)], \\ w_{i+1}(n+1)=w_{i+1}(n)-2\mu_i q_2'(n)x_{(i+1)w}(n) \\ \qquad +\eta_i[w_{i+1}(n)-w_{i+1}(n-1)]. \end{cases} \tag{22}$$

The introduction of the momentum factor means that when the weight coefficient changes are large at the current moment, the correction amount of the weight coefficients at the current moment increases. This can help the algorithm achieve faster convergence speed in the initial stage and accelerate the gradient descent process when the error signal undergoes sudden changes. The introduction of the momentum factor expands the range of the algorithm's step size, reducing the sensitivity of the step size to the aggregation degree of the reference signal autocorrelation matrix's eigenvalues, which helps the algorithm better converge. Compared with other variable step size algorithms, the introduction of the momentum factor does not bring too much computation, and the upper and lower bounds of the momentum factor are determined, which can effectively improve the convergence speed and tracking performance of the system.

3 Numerical Results and Discussion

This paper aims to enhance the effectiveness of the algorithm and highlight the nonlinear vibration characteristics of gear systems. To achieve this goal, we have reduced both the mesh damping and support damping beyond the existing theoretical basis. The modified damping of the gear system is demonstrated in Figure 4, which presents the bifurcation diagram.

From Figure 4, it is shown that the diagram reveals the presence of periodic motion in the low frequency band of the gear, whereas chaotic or quasi periodic motions occur in the middle and high frequencies. Meanwhile, the spectrum waterfall diagram illustrates that the gears exhibit varying motion states based on the excitation frequency. The analysis is performed for different motion states.

3.1 Analysis of Vibration Reduction Effect of the FxLMS Algorithm

When the excitation frequency is 0.52, the system is in a period-1 motion. As shown in Figure 5, after convergence, the time domain of the system displays vibration stability and exhibits a clearly periodic behavior according to the local magnification diagram. Additionally, the FFT spectrum of the system indicates peak frequencies at 1, 2, and 3, corroborating that the system is experiencing a periodic motion. The effect of vibration reduction is presented in Figure 5. When FxLMS algorithm is applied for the gear transmission system and the step size is set to 1×10^{-3}. It is evident that the FxLMS algorithm effectively reduces vibrations in the time domain waveform while

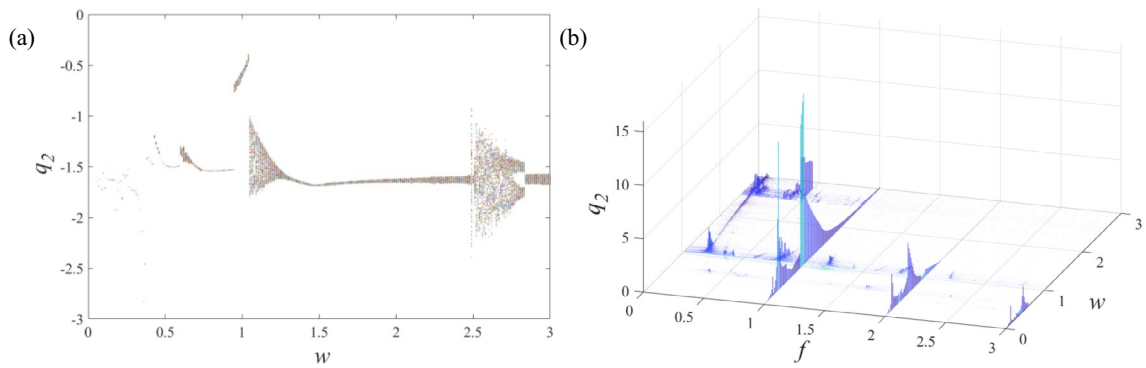

Figure 4 (**a**) Bifurcation diagram and (**b**) spectrum waterfall diagram of the gear pair with different excitation frequencies

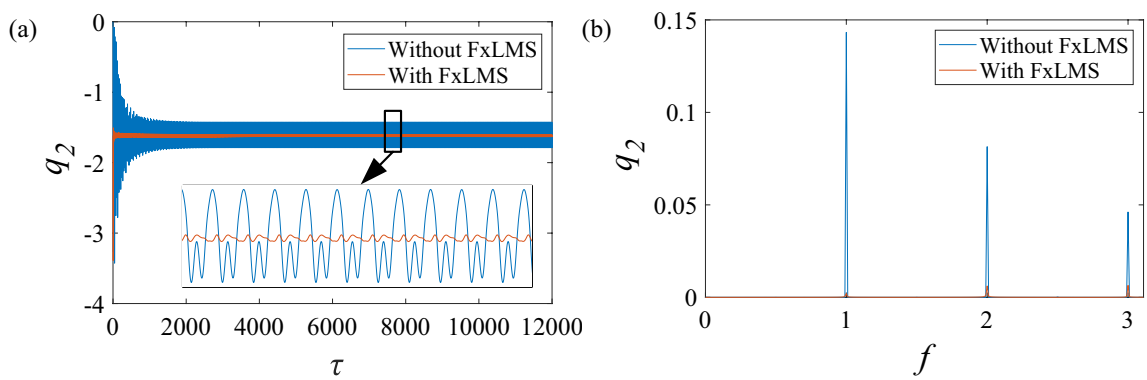

Figure 5 Dynamic response of the gear system at 0.52 when the step size is set to 1×10^{-3}: (**a**) Time domain (**b**) FFT spectrum

also significantly shortening the convergence time. The peak in the FFT spectrum is also greatly reduced, and there are no other sidebands present. These results demonstrate that for periodic vibration, the FxLMS algorithm can effectively reduce vibrations and increase the stability of the gear system during vibration.

When the step size is set to 1×10^{-6}, the time domain and FFT spectrum of the gear system are shown in Figure 6. In the time domain, it is apparent that the FxLMS algorithm causes a shift in the vibration signal relative to the original signal during the start-up process, and the damping effect becomes less noticeable once the vibration stabilizes. In the FFT spectrum, a certain decrease in the peak value of the vibration signal can be observed when the FxLMS algorithm is applied. The results indicate that the algorithm has a slight reduction effect for a step size of 1×10^{-6}, but the reduction effect is markedly reduced compared to that for a step size of 1×10^{-3}.

As the excitation frequency is 1.05, it is evident that the waveforms display consistency in the time domain, but the amplitude of each cycle varies and converges at a slower pace. Moreover, the FFT spectrum presents discontinuous peaks in several locations, suggesting that the system exhibits quasi-periodic motion. Techniques such as active vibration control and condition monitoring are often employed to identify and mitigate quasi-periodic motion in gear systems.

In Figure 7, it can be seen that the FxLMS algorithm has a significant damping effect on the quasi-periodic vibration state when the step size is set to 1×10^{-3}. The amplitude of the waveform in the time domain is effectively reduced, and there is a significant decrease in the peak value in the FFT spectrum. These results highlight the clear and noticeable damping effect of the FxLMS algorithm at this particular step size for the quasi-periodic motion state.

As shown in Figure 8, for a step size of 1×10^{-6}, the time domain shows that the starting phase still displays an offset, but the effect of vibration reduction improves gradually over time. In the FFT spectrum, there is a significant reduction in the peak at frequency 1. Comparing with Figure 6, it suggests that the FxLMS algorithm provides better damping for the quasi-periodic motion state than the periodic motion state at a step size of 1×10^{-6}.

Figure 9 displays the time domain and FFT spectrum when the excitation frequency reaches 2.49. The time domain shows a waveform that is complex, and the motion state is irregular and unpredictable. Meanwhile,

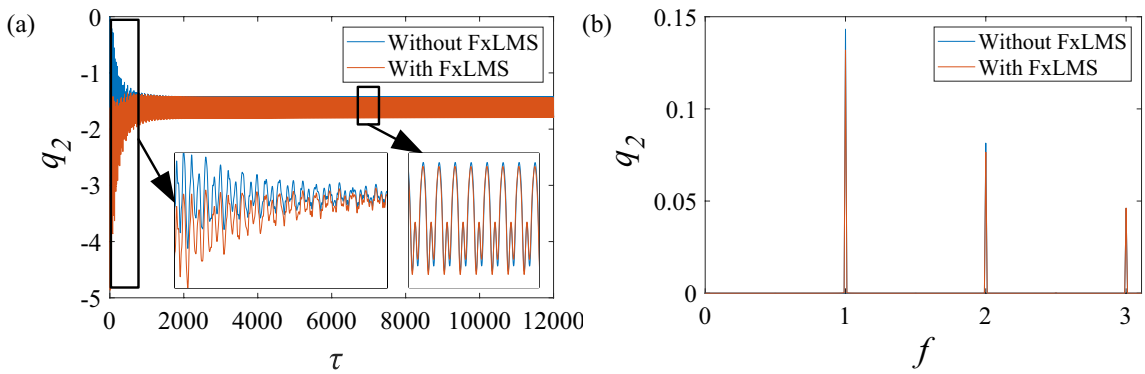

Figure 6 Dynamic response of the gear system at 0.52 when the step size is set to 1×10^{-6}: (**a**) Time domain (**b**) FFT spectrum

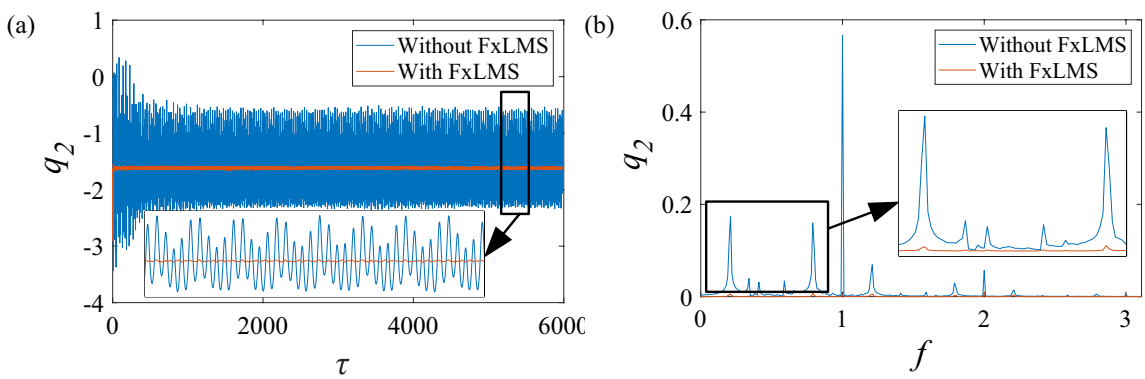

Figure 7 Dynamic response of the gear system at 1.05 when the step size is set to 1×10^{-3}: (**a**) Time domain, (**b**) FFT spectrum

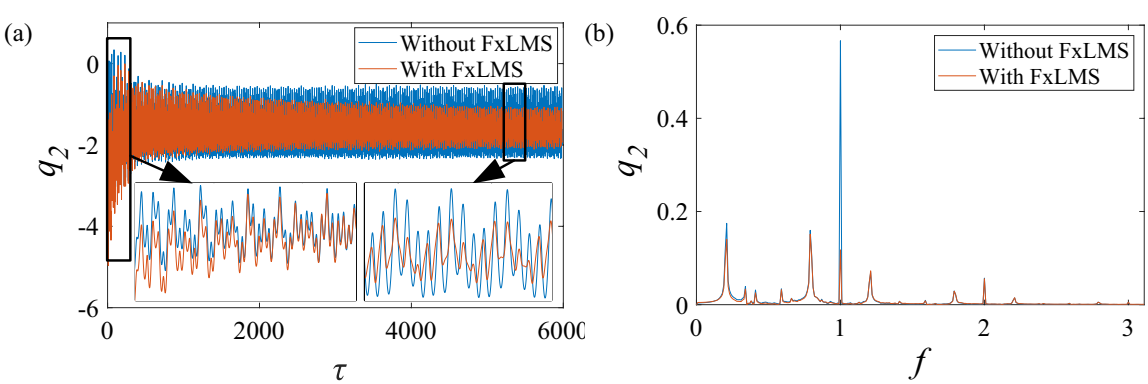

Figure 8 Dynamic response of the gear system at 1.05 when the step size is set to 1×10^{-6}: (**a**) Time domain, (**b**) FFT spectrum

the continuous peaks in the FFT spectrum signify that the gear system is in a chaotic state at this time. Chaotic motion in a gear system can lead to reduced system efficiency, increased noise levels, and mechanical failure over time. Therefore, it is necessary to reduce the vibration when the gear system is in a chaotic motion state.

Based on Figure 10, it can be observed that the time domain diverges, indicating that the step size of 1×10^{-3} is not capable of providing effective damping to the system under a chaotic motion state, and may even result in severe consequences. Consequently, this step size is unsuitable for the present application.

As displayed in Figure 11, when the step size is reduced to 1×10^{-6}, it can be observed that the vibration in the time domain, based on the FxLMS algorithm for damping, no longer diverges and provides better damping. In the FFT spectrum, there is also a significant reduction in the peak value. This conclusion indicates that the FxLMS

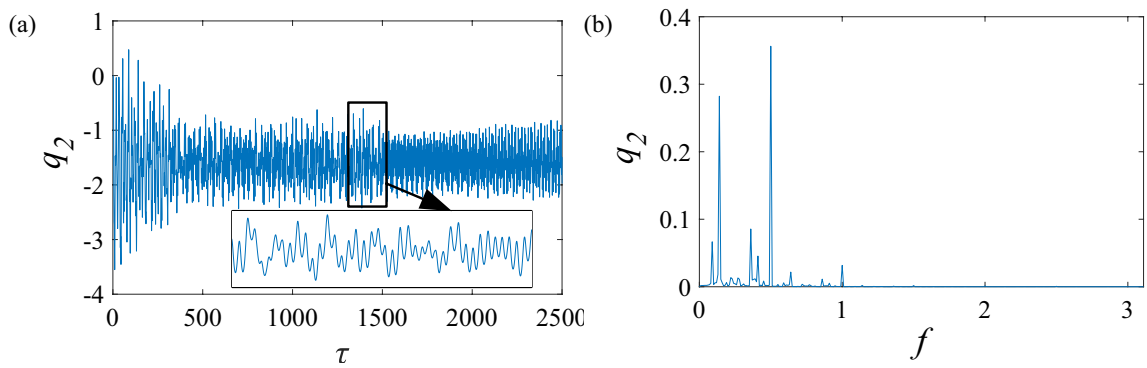

Figure 9 Dynamic response of the gear system at 2.49: (**a**) Time domain (**b**) FFT spectrum

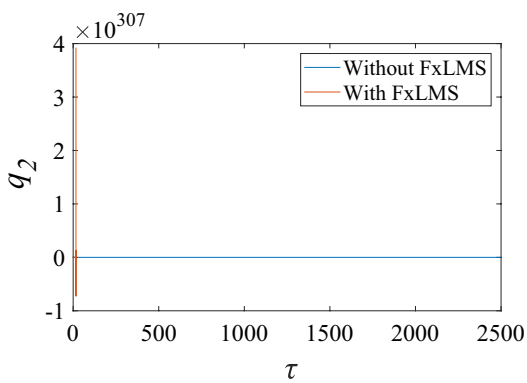

Figure 10 Time domain of the gear system at 2.49 when the step size is set to 1×10^{-3}

algorithm provides more prominent damping in the chaotic motion state of the gear system, with a step size of 1×10^{-6}.

The effects of different momentum factors on damping are presented in Figure 12. Dividing the time domain into 40 groups, Figure 12(b), (d), and (f) illustrate the root mean square (RMS) values for each group. As shown in Figure 12, larger momentum factors generally result in better damping effects, especially for complex motion states in gear systems. However, excessively large momentum factors can lead to system instability and reduced resistance to external disturbances. Figure 13 demonstrates that with a step size of 1×10^{-3}, increasing the momentum factor to 0.8 initially improves the system's vibration reduction. However, as time passes, the vibrations start to disperse and the system becomes unstable. Therefore, selecting an appropriate momentum factor and step size can significantly improve the damping of gear systems.

3.2 Analysis of Vibration Reduction Effect of the VSMFxLMS Algorithm

To verify the performance of the variable-step active damping algorithm, combining momentum factors, which was proposed in the paper to improve the performance of the combined algorithm, a comparison will be made with the FxLMS algorithm. The comparison will focus on the results of both algorithms to see which algorithm performs better in terms of active damping.

Based on the results shown in Figure 14(a), it can be observed that the damping effect of the VSMFxLMS

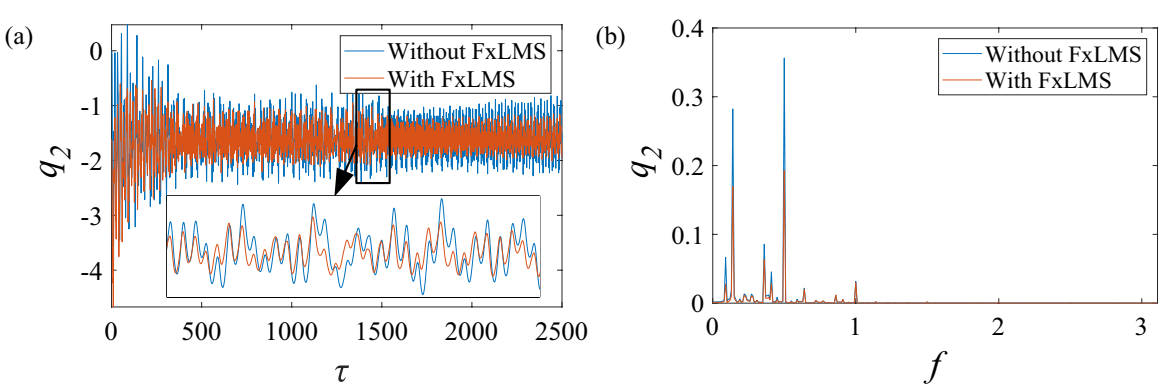

Figure 11 Dynamic response of the gear system at 2.49 when the step size is set to 1×10^{-6} (**a**) Time domain (**b**) FFT spectrum

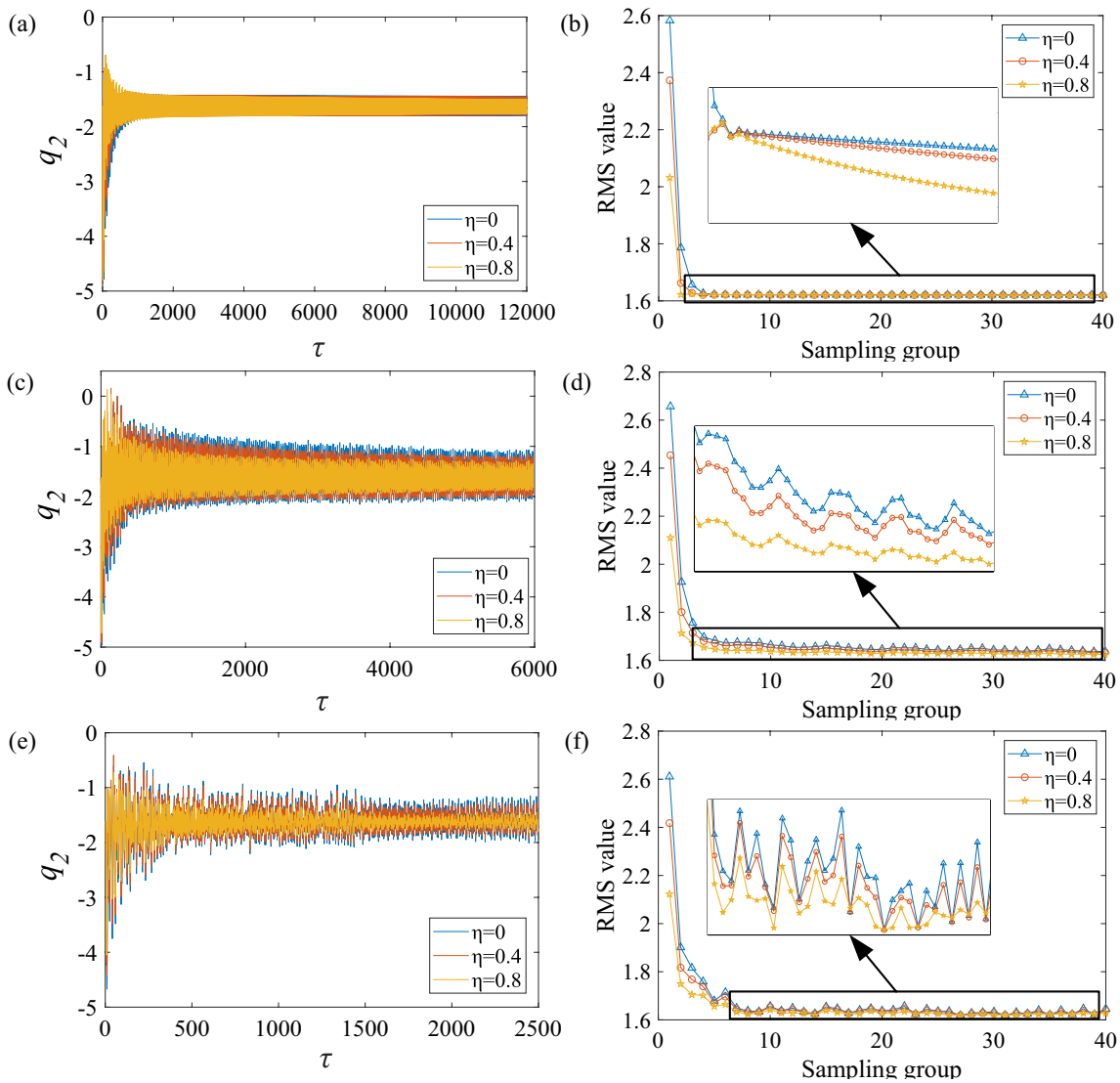

Figure 12 Time domains (**a**), (**c**), (**e**) and RMS values (**b**), (**d**), (**f**) at different excitation frequency when the step size is set to 1×10^{-6} (**a**), (**b**) 0.52 (**c**), (**d**) 1.05 (**e**), (**f**) 2.49

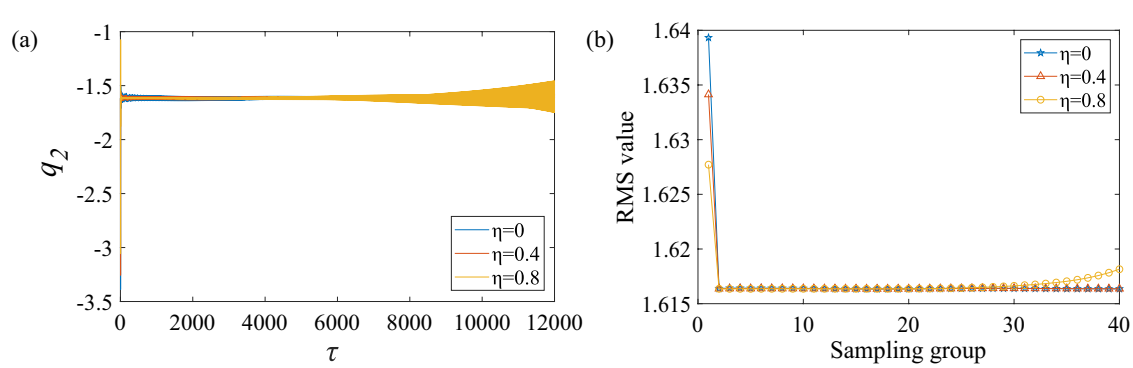

Figure 13 (**a**) Time domains and (**b**) RMS values at the excitation frequency 0.52 when the step size is set to 1×10^{-3}

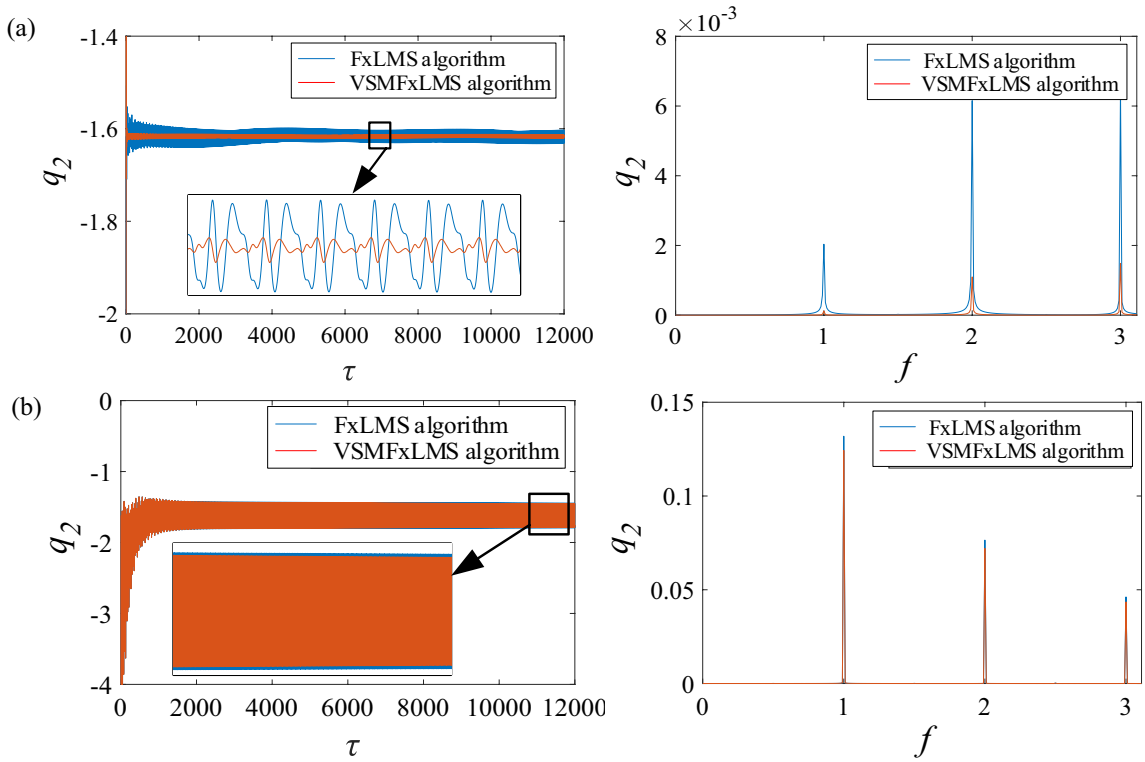

Figure 14 Comparison of different algorithms at excitation frequency of 0.52 when the step size is set to (**a**) 1×10^{-3} (**b**) 1×10^{-6}

algorithm improves significantly. Moreover, in the FFT spectrum, the peak of the VSMFxLMS algorithm significantly decreases, indicating that the damping effect of the VSMFxLMS algorithm is better than that of the optimized FxLMS algorithm. This comparison demonstrates the superior performance of the proposed variable-step active damping algorithm with momentum factors, and its effectiveness in reducing peak values and improving damping effects. However, in Figure 14(b), the reduction effect of the VSMFxLMS algorithm is not obvious. It shows that the reduction effect of the VSMFxLMS algorithm on the gear system is also directly related to the step size.

The reduction effect of different step sizes for the excitation frequency of 1.05 is shown in Figure 15. Similarly to the excitation frequency of 0.52, the VSMFxLMS algorithm shows good damping effect and fast convergence speed at a step size of 0.1, resulting in a significant decrease in the amplitude of the time domain and the peak of the FFT spectrum. At a step size of 1×10^{-6}, the damping effect of the VSMFxLMS algorithm is not as significant as that for the step size of 1×10^{-3}. However, it can be concluded that the VSMFxLMS algorithm generally optimizes the FxLMS algorithm better for quasi-periodic motion states compared to periodic motion states. These results suggest that the proposed variable-step active damping algorithm with momentum factors has the potential to improve damping performance for various types of vibrations.

The optimization results for the algorithm with an excitation frequency of 2.49 are presented in Figure 16. The algorithm does not converge at a step size of 1×10^{-3}, so only the optimization results at a step size of 1×10^{-6} are compared. It can be observed that the convergence speed and amplitude of the VSMFxLMS algorithm have significantly improved. Additionally, the peak in the FFT spectrum is significantly reduced, but the sidebands show little change. This suggests that there is a significant improvement in the amplitude during the gear system vibration, but the motion state remains almost the same. The findings of Figures 14 and 15 also support this conclusion.

Overall, the proposed algorithm optimizes better when the gear motion state is more complex, which aligns with the intention of designing an optimization algorithm. This result indicates that the proposed algorithm has the potential to improve the damping performance of gear systems with complex vibration patterns. However, compared with the FxLMS algorithm, the VSMFxLMS algorithm with drive exhibits greater fluctuations when the error sensor signal is disturbed, and the convergence of the large magnitude is weaker than the FxLMS algorithm

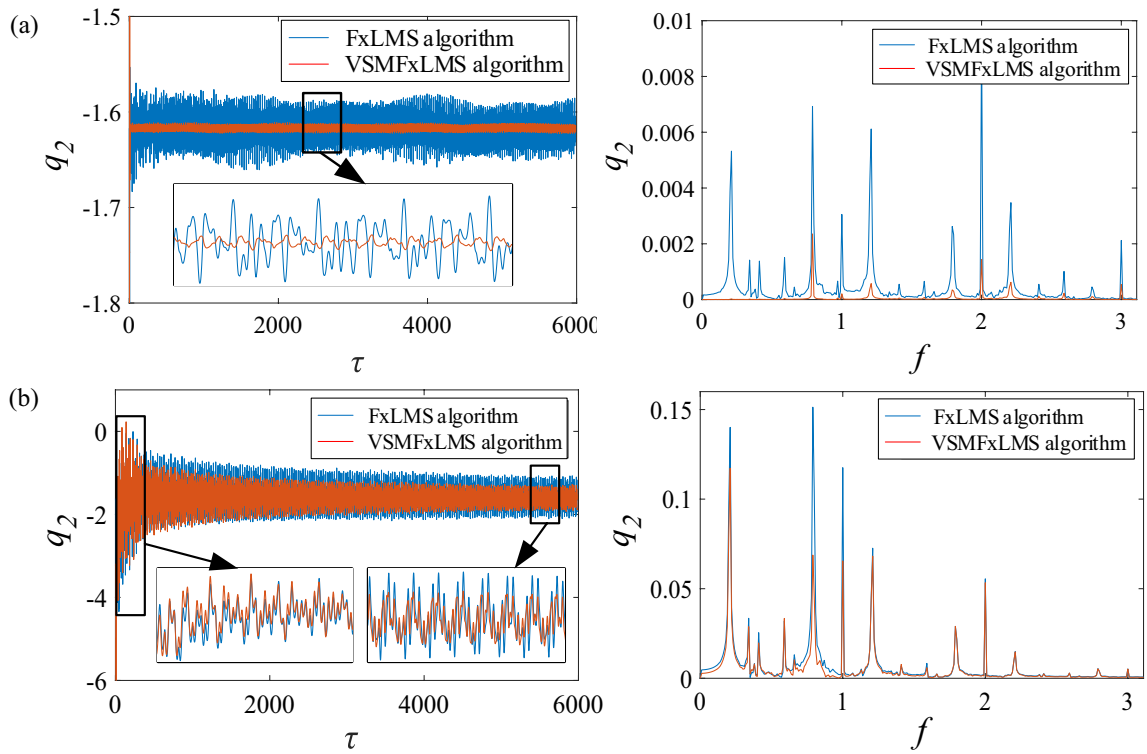

Figure 15 Comparison of different algorithms at excitation frequency of 1.05 when the step size is set to (**a**) 1×10^{-3} (**b**) 1×10^{-6}

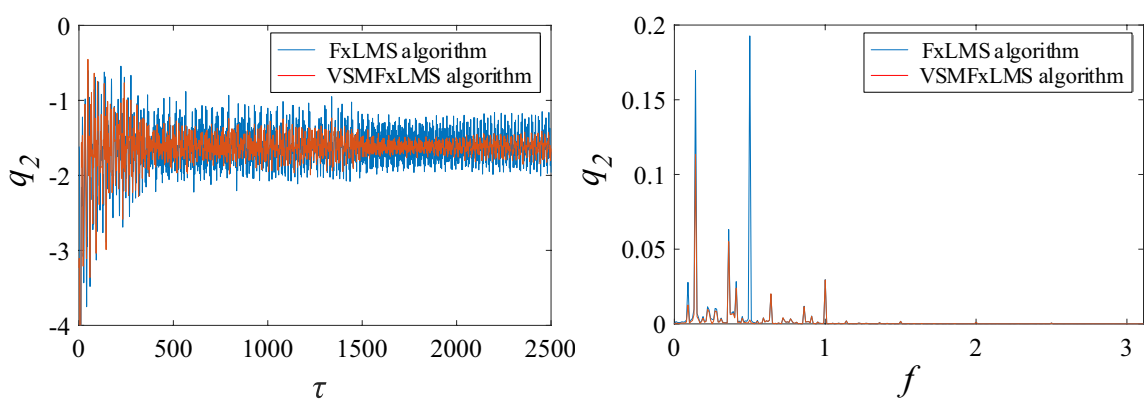

Figure 16 Comparison of different algorithms at excitation frequency of 2.49 when the step size is set to 1×10^{-6}

after the perturbation, but when it tends to stabilize, the VSMFxLMS algorithm with drive has a significantly better convergence performance than the FxLMS algorithm.

4 Conclusions

This paper proposes a multi-channel VSMFxLMS algorithm based on the FxLMS algorithm, which considers the momentum factor to achieve active damping in the gear system's vibration process. The study analyzes the nonlinear dynamic response characteristics of the gear system and draws the following conclusions:

(1) The gears demonstrate different dynamic characteristics at varying excitation frequencies. The FxLMS algorithm is effective in damping the gears. The damping effect at step size 1×10^{-3} is significantly optimized compared to that at a step size of 1×10^{-6}. However, when the gear system is in chaotic motion, a step size of 1×10^{-3} leads to vibration scat-

tering. Therefore, choosing an appropriate step size is crucial for gear damping using the FxLMS algorithm.

(2) The damping effect of the gear system is typically more pronounced with a larger momentum factor. However, if the momentum factor reaches 0.8, the gear system's vibrations may become unstable or even scatter. Thus, both the momentum factor and step length must be appropriately selected simultaneously.

(3) The multi-channel active vibration reduction algorithm design is optimized for steady-state error and convergence speed. The adaptive filter power coefficient updates are performed by combining the momentum factor's skip-tongue line variable step size. The experimental results show that the multi-channel combination algorithm effectively reduces gear system vibrations when combined with the FxLMS algorithm.

Acknowledgements
Not applicable.

Author Contributions
ZG is mainly responsible for the writing of articles; MC and YW are mainly responsible for checking the articles; ZG, YK and KX are responsible for funding. All authors read and approved the final manuscript.

Funding
Supported by Sichuan Provincial Science and Technology Program (Grant No. 2024NSFSC0902), National Natural Science Foundation of China (Grant Nos. 52405254, 52105108, 52375039), the Young Elite Scientists Sponsorship Program by CAST (Grant No. 2023QNRC001), Hebei Provincial Natural Science Foundation (Grant No. E2023105039).

Data availability
The data are available from the corresponding author on reasonable request.

Declarations

Competing Interests
The authors declare no competing financial interests.

Received: 8 October 2023 Revised: 11 September 2024 Accepted: 14 September 2024
Published online: 12 October 2024

References

[1] D Richards, D J Pines. Passive reduction of gear mesh vibration using a periodic drive shaft. *Journal of Sound and Vibration*, 2003, 264(2): 317-342.
[2] M Hui, P Xu, R Feng, et al. Evaluation of optimum profile modification curves of profile shifted spur gears based on vibration responses. *Mechanical Systems and Signal Processing*, 2016, 70-71: 1131-1149.
[3] W Xiao, J Li, S Wang, et al. Study on vibration suppression based on particle damping in centrifugal field of gear transmission. *Journal of Sound and Vibration*, 2016, 366: 62-80.
[4] W Xiao, Y Huang, H Jiang, et al. Effect of powder material on vibration reduction of gear system in centrifugal field. *Powder Technology*, 2016, 294: 146-158.
[5] W Xiao, Z Xu, F Zhang, et al. Effect of particle damping on high-power gear transmission with dynamic coupling for continuum and non-continuum. *Applied Acoustics*, 2021, 173: 107724.
[6] W Yu, CK Mechefske, M Timusk. Influence of the addendum modification on spur gear back-side mesh stiffness and dynamics. *Journal of Sound and Vibration*, 2017, 389: 183-201.
[7] J Wei, A Zhang, D Qin, et al. A coupling dynamics analysis method for a multistage planetary gear system. *Mechanism and Machine Theory*, 2017, 110: 27-49.
[8] J Wei, A Zhang, G Wang, et al. A study of nonlinear excitation modeling of helical gears with modification: Theoretical analysis and experiments. *Mechanism and Machine Theory*, 2018, 128: 314-335.
[9] K Lu, L He, W Yan. Experimental study of IERSFDs for vibration reduction of gear transmissions. *Journal of Vibroengineering*, 2019, 21(2): 409-419.
[10] FS Samani, M Molaie, F Pellicano. Nonlinear vibration of the spiral bevel gear with a novel tooth surface modification method. *Meccanica*, 2019, 54: 1071-1081.
[11] C Wang. Multi-objective optimal design of modification for helical gear. *Mechanical Systems and Signal Processing*, 2021, 157: 107762.
[12] H Jiang, F Liu. Dynamic modeling and analysis of elastic isolation damping gears. *Journal of Vibroengineering*, 2022, 24(4): 637-650.
[13] X Chen, J Wei, J Zhang, et al. A novel method to reduce the fluctuation of mesh stiffness by high-order phasing gear sets: Theoretical analysis and experiment. *Journal of Sound and Vibration*, 2022, 524: 116752.
[14] C Gill-Jeong. Nonlinear behavior analysis of spur gear pairs with a one-way clutch. *Journal of Sound and Vibration*, 2007, 301: 760-776.
[15] W Gao, L Wang, Y Liu. A modified adaptive filtering algorithm with online secondary path identification used for suppressing gearbox vibration. *Journal of Mechanical Science and Technology*, 2016, 30(11): 4833-4843.
[16] R P Spada, R Nicoletti. Application of the Udwadia–Kalaba methodology to the active control of shaft vibration. *Journal of Vibration and Control*, 2017, 23(13): https://doi.org/10.1177/1077546315611003
[17] C U Dogruer, A K Pirsoltan. Active vibration control of a single-stage spur gearbox. *Mechanical Systems and Signal Processing*, 2017, 85: 429-444.
[18] W Sun, F Zhang, W Zhu, et al. A comparative study based on different control algorithms for suppressing multistage gear transmission system vibrations. *Shock and Vibration*, 2018: 7984283.
[19] H Wang, F Zhang, H Li, et al. Experimental analysis of an active vibration frequency control in gearbox. *Shock and Vibration*, 2018: 1402697.
[20] P Zech, D F Ploeger, S Rinderknecht. Active control of planetary gearbox vibration using phase-exact and narrowband simultaneous equations adaptation without explicitly identified secondary path models. *Mechanical Systems and Signal Processing*, 2019, 120(Apr.1): 234-251.
[21] L Sheng, W Li, Y Wang, et al. Nonlinear dynamic analysis and chaos control of multi-freedom semi-direct gear drive system in coal cutters. *Mechanical Systems and Signal Processing*, 2019, 116: 62-77.
[22] S Luo, F Zhang, C Liu, et al. Frequencies estimation of gearbox vibration signal based on normalized lattice filter with RLS-based algorithm. *Measurement Science and Technology*, 2021, 32(1): 015104.
[23] X Peng, J Zhou. Optimization design for dynamic characteristics of face gear drive with surface-active modification. *Mechanism and Machine Theory*, 2022, 176: 105007.
[24] D Zhang, C Guan. Active vibration control of robot gear system based on adaptive control algorithm. *Journal of Sensors*, 2022: 1-8.
[25] G Majumder, R Tiwari. Experimental study on vibration control of spur geared rotor system with active magnetic bearings. *Journal of Sound and Vibration*, 2022, 532: 117005.
[26] K Olanipekun, E Rustighi, N Ferguson. Simulation study of active vibration control of planetary gear: Theoretical and numerical analysis using pole placement. *Journal of Low Frequency Noise, Vibration and Active Control*, 2023, 42(4): 1543-1559.
[27] Z Geng, J Li, K Xiao, et al. Analysis on the vibration reduction for a new rigid–flexible gear transmission system. *Journal of Vibration and Control*, 2022, 28(17-18): 2212-2225.
[28] J Li, G Liu, S Zheng, et al. Micro-jitter control of magnetically suspended control moment gyro using adaptive LMS algorithm. *IEEE/ASME Transactions on Mechatronics*, 2021, 27(1): 327-335.

Zhibo Geng born in 1992, is currently a postdoctoral at *School of Aeronautics and Astronautics, University of Electronic Science and Technology of China, China*. He received his PhD degree from *Chognqing University, China*, in 2020. His research interests include dynamic and control of the transmission system.

Min Chen born in 1974, is currently a professor at *University of Electronic Science and Technology of China, China*. He received his PhD degree from *University of Electronic Science and technology of China, China*, in 2008.

Yingjian Wang born in 1998, received his Master's Degree from *School of Aeronautics and Astronautics*, *University of Electronic Science and Technology of China, China*, in 2023. His research interests are in the area of sound control and optimization algorithm.

Yun Kong born in 1992, is currently an associate professor with *School of Mechanical Engineering, Beijing Institute of Technology, China*. He received his Ph.D. degree in Mechanical Engineering from *Tsinghua University, China*, in 2020.

Ke Xiao born in 1978, is currently an associate professor with *College of Mechanical and Vehicle Engineering, Chongqing University, China*. He received his Ph.D. degree in Mechanical Engineering from *Chognqing University, China*, in 2013.